
Motion Prediction of Traffic Actors for Autonomous Driving using Deep Convolutional Networks

Nemanja Djuric, Vladan Radosavljevic, Henggang Cui,
Thi Nguyen, Fang-Chieh Chou, Tsung-Han Lin, Jeff Schneider
Uber Advanced Technologies Group
{ndjuric, vradosavljevic, hcui2, thi, fchou, hanklin, jschneider}@uber.com

Abstract

Recent algorithmic improvements and hardware breakthroughs resulted in a number of success stories in the field of AI impacting our daily lives. However, despite its ubiquity AI is only just starting to make advances in what may arguably have the largest impact thus far, the nascent field of autonomous driving. In this work we discuss this important topic and address one of crucial aspects of the emerging area, the problem of predicting future state of autonomous vehicle's surrounding necessary for safe and efficient operations. We introduce a deep learning-based approach that takes into account current state of traffic actors and produces rasterized representations of each actor's vicinity. The raster images are then used by deep convolutional models to infer future movement of actors while accounting for inherent uncertainty of the prediction task. Extensive experiments on real-world data strongly suggest benefits of the proposed approach. Moreover, following successful tests the system was deployed to a fleet of autonomous vehicles.

1 Introduction

Recent years have witnessed unprecedented advances in Artificial Intelligence (AI) applications, with a number of highly publicized success stories that have captured attention and imagination of professionals and laymen alike. Computers have reached and even surpassed human performance in centuries old games such as go and chess [33, 34], are starting to understand health conditions and suggest medical treatment [38], and can even reason about complex relationships conveyed through images [39]. Prior to this, AI was already well-established at the very core of multibillion-dollar industries such as advertising [5] and finances [26], where algorithmic approaches have all but replaced human experts. Nevertheless, despite huge strides the AI revolution is far from over [12]. One of the major industries mostly untouched by the ongoing progress is the automobile domain, where AI may potentially make its greatest impact yet through the advent of self-driving cars.

Driving a motor vehicle is a complex undertaking, requiring drivers to understand involved multi-actor scenes in real time and act upon rapidly changing environment within a fraction of a second (*actor* is a generic term referring to any surrounding vehicle, pedestrian, bicycle, or other potentially moving object). Unfortunately, humans are famously ill-fitted for the task. This is sadly corroborated by grim road statistics that often worsen year after year, showing that traffic accidents were the number four cause of death in the US in 2015, accounting for more than 5% of the total [24]. In addition, despite large investments by governments and progress made in traffic safety technologies, 2017 was still one of the deadliest years for motorists in the past decade [25]. Moreover, human error is considered responsible for up to 94% of car crashes [36], strongly suggesting that mitigating or even removing the unreliable human factor could potentially save hundreds of thousands of motorists' lives and tens of billions of dollars in accident-related damages and medical expenses [4].

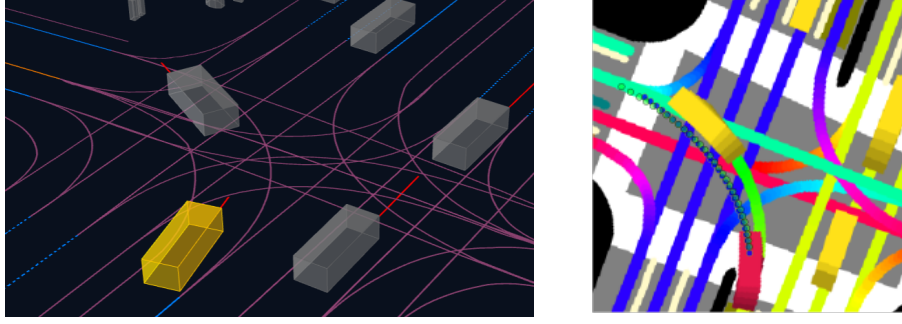


Figure 1: Example of a complex scene handled by our model; (a) scene in a 3D viewer, with indicated actor of interest; (b) rasterized surrounding in bird’s eye view of the actor of interest (colored red) used as an input to CNN, with overlaid trajectories (dotted green line - ground truth; blue - predicted)

Latest advances in AI and breakthroughs in high-performance computing, allowing for more powerful processing hardware at lower costs, unlocked the potential to reverse the regrettable negative trend of safety on our public roads. In particular, together they gave rise to development of self-driving technology, where driving decisions are entrusted to a computer aboard an autonomous vehicle (AV), equipped with a number of external sensors and capable of processing large amounts of information at speeds and throughputs far surpassing human capabilities. Once fully matured the technology is expected to drastically improve road safety and redefine the very way we organize transportation and even our lives [29]. To this end, the industry and governments are working together to fulfill this potential and bring the AVs to consumers, with front-runners such as Waymo, Uber, and Ford investing significant resources into autonomous research, and states such as Arizona, Nevada, and California enacting necessary legal frameworks. Nevertheless, autonomous driving is still in its initial phases of development, with a number of challenges lying ahead of the researchers.

To safely deploy AVs to public roads one must solve a sequence of tasks that include detection and tracking of actors in AV’s surrounding, predicting their future trajectories, as well as navigating the AV safely and effectively towards its intended destination while taking into account current and future states of the actors. In this work we focus on a critical component of this pipeline, predicting future trajectory of tracked vehicles (in the following we use the terms *vehicle* and *actor* interchangeably), where a working detection and tracking system is assumed. Our main contributions are as follows:

- We propose to rasterize surrounding of each vehicle in AV’s vicinity, thus providing full context and information necessary for accurate future trajectory prediction;
- We trained deep convolutional neural network (CNN) to predict future vehicle trajectories, while accounting for inherent uncertainty of vehicle motion in road traffic;
- We run evaluation on large-scale real-world data showing that the system provides accurate predictions and well-calibrated uncertainties, clearly indicating its practical benefits;
- Following extensive testing in both offline and online setting, the system was successfully deployed to a fleet of self-driving vehicles.

Example of a complex scene handled by our model is shown in Figure 1. Figure 1(a) shows the scene in an internal 3D viewer, while Figure 1(b) shows the corresponding rasterized 2D input image (or *raster*) and the predicted trajectory (we refer to the actor being considered and whose surrounding corresponds to the input raster as *actor of interest*). The method uses rasterized vehicle context (including map and other actors) to accurately predict actor’s movement in a dynamic environment.

2 Related work

In the past decade a number of methods were proposed to tackle the problem of predicting future motion of traffic actors. Comprehensive overview of the topic can be found in [23, 43]. Here, we review literature from the perspective of autonomous driving. We first cover engineered approaches commonly used in practice in the self-driving industry. Then, we discuss learned approaches using classical machine learning methods as well as deep learning.

2.1 Motion prediction in self-driving systems

Accurate prediction of actors' motion is a critical component of an effective self-driving system [7, 46]. In particular, prediction is tightly coupled with AV's egomotion planning, as it is essential to accurately estimate future world state in order to correctly plan AV's path through a highly dynamic environment. Inaccurate motion prediction may lead to accidents, as exemplified by a collision between MIT's "Talos" and Cornell's "Skyne" during the 2007 DARPA Urban Challenge [8].

Most of the deployed self-driving systems use well-established engineered approaches for motion prediction. The common approach consists of computing object's future motion by propagating its state over time based on kinematics and assumptions of underlying physical system. State estimate usually comprises position, speed, acceleration, and heading of the object, and techniques such as Kalman filter (KF) [15] are used to estimate and propagate the state in the future. For example, in Honda's deployed system [7], KF tracker is used to predict motion of vehicles around AV. While this approach works well for short-term predictions, its performance degrades for longer horizons as the model ignores surrounding context (e.g., roads, other actors, traffic rules). On the other hand, Mercedes Benz's motion prediction component uses map information as a constraint to compute vehicle's future position [46]. The system first associates each detected vehicle with one or more lanes from the map. Then, all possible paths are generated for each (*vehicle, associated lane*) pair based on map topology, lane connectivity, and vehicle's current state estimate. This heuristic provides reasonable predictions in common cases, however it does not scale well and is not able to model unusual traffic scenarios. As an alternative to existing deployed engineered approaches, by considering large amounts of training data our proposed approach automatically learns the fact that vehicles usually obey road and lane constraints, while being capable of also handling outliers.

2.2 Learned prediction models

Manually designed engineered models often impose unrealistic assumptions not supported by the data (e.g., that traffic always follows designated lanes), which motivated use of learned models as an alternative. A large class of learned models are maneuver-based models (e.g., using Hidden Markov Model [37]) which are object-centric approaches that predict discrete action of each object independently. The independence assumption does not often hold true, which is mitigated by the use of Bayesian networks [31] that are computationally more expensive and not feasible in real-time tasks. Additionally, in [3] authors learned scene-specific motion patterns and applied them to novel scenes with an image-based similarity function. However, these methods also require manually designed features to capture context information, resulting in suboptimal performance. Alternatively, Gaussian Process (GP) regression can be used to address the motion prediction problem [41]. GP regression is well-suited for the task with desirable properties such as ability to quantify uncertainty, yet it is limited when modeling complex actor-environment interactions. In recent work researchers focused on how to model environmental context using Inverse Reinforcement Learning (IRL) [45]. Kitani *et al.* [18] used inverse optimal control to predict pedestrian paths by considering scene semantics, however the proposed IRL methods are inefficient for real-time applications.

The success of deep learning [11] motivated its use for motion prediction. In [22] a Recurrent Neural Network (RNN)-based method was proposed for long-term predictions of multiple interacting agents given scene context. In [2] authors proposed a social Long Short-Term Memory (LSTM) to model human movement together with social interactions. Authors of [9] used LSTM to predict ball motion in billiards using a sequence of visual glimpses. In [42] LSTMs were used to classify basketball plays, with overhead raster images as inputs. Similarly, the authors of [27, 28] used overhead raster as input to RNNs to predict raster image of a scene in a next timestep, unlike our work where per-object trajectories are directly inferred. Due to strict time constraints of a deployed real-time system, as well as a requirement to more easily debug and understand model decisions made on public roads, we used simpler feed-forward CNN architectures for the task of motion prediction.

3 Proposed approach

Let us assume that we have access to real-time data streams coming from sensors such as lidar, radar, or camera, installed aboard a self-driving vehicle. Furthermore, we assume to have an already functioning tracking system ingesting the sensor data, allowing detection and tracking of traffic actors in real-time. For example, we can make use of any of a number of Kalman filter-based methods that

have found wide practical use [6], taking sensor data as input and outputting tracks of individual actors that represent their state estimates at fixed intervals. State estimates contain the following information describing an actor: bounding box, position, velocity, acceleration, heading, and heading change rate. Lastly, we assume access to mapping data of an area where the AV is operating, comprising road and crosswalk locations, lane directions, and other relevant map information.

Let us denote overall map data by \mathcal{M} , and a set of discrete times at which tracker outputs state estimates as $\mathcal{T} = \{t_1, t_2, \dots, t_T\}$, where time gap between consecutive time steps is constant (e.g., gap is equal to $0.1s$ for tracker running at frequency of $10Hz$). Then, we denote state output of a tracker for the i -th actor at time t_j as \mathbf{s}_{ij} , where $i = 1, \dots, N_j$ with N_j being a number of unique actors tracked at t_j . Note that in general the actor counts vary for different time steps as new actors appear within and existing ones disappear from the sensor range. Then, given data \mathcal{M} and all actors' state estimates up to and including time step t_j (denoted by \mathcal{S}_j), the task is to predict sequence of future states $[\mathbf{s}_{i(j+1)}, \dots, \mathbf{s}_{i(j+H)}]$, where H denotes the number of future consecutive time steps for which we predict states (or *prediction horizon*). Without the loss of generality, in this work we simplify the task to infer i -th actor's future positions instead of full state estimates, denoted as $[x_{i(j+1)}, \dots, x_{i(j+H)}]$ for x -positions and $[y_{i(j+1)}, \dots, y_{i(j+H)}]$ for y -positions. Past and future positions at time t_j are represented in actor-centric coordinate system derived from actor's state at time t_j , where forward direction represents x -axis, left-hand direction represents y -axis, and actor's bounding box centroid represents the origin.

3.1 Model inputs

To model dynamic actor context at time step t_j we use state data \mathcal{S}_j , comprising actors' states until t_j , inclusive. In addition, to model static context we use map data \mathcal{M} , comprising road and crosswalk polygons, as well as lane directions and boundaries. Road polygons describe drivable surface, lane describes driving path for a single vehicle, while crosswalk polygons describe road surface used for pedestrian crossing. Lanes are represented by boundaries and directed lines positioned at the center.

Instead of manually defining features that represent context for each individual actor, we propose to rasterize scene for the i -th actor at time step t_j into an RGB image (see Figure 1 for example). Then, we train CNN using rasterized images as inputs to predict actor's trajectory, where the network automatically infers relevant features. Optionally, the model can also take as input a current state of the actor of interest \mathbf{s}_{ij} represented as a vector (see Section 3.3 for details of the architecture).

3.1.1 Rasterization

To describe rasterization, let us first introduce a concept of *vector layer*, formed by a collection of polygons and lines that belong to a common type. For example, in the case of map elements we have vector layer of roads, of crosswalks, and so on. To rasterize vector layer into an RGB space, each vector layer is manually assigned a color from a set of distinct RGB colors that make a difference among layers more prominent. The only layer that does not have its defined RGB color is a layer that encodes lane direction. Instead of assigning a specific RGB color, we use a direction of each straight line segment as hue value in HSV color space, with saturation and value set to maximum. We then convert HSV to RGB color space, thus encoding driving direction of each lane in the resulting rasterized image. For example, in Figure 1 we can see that lanes going in opposite directions are represented by colors diametrically opposite to each other on the HSV color cylinder. Once the colors are defined, vector layers are rasterized one by one on top of each other, in the order from layers that represent larger areas such as road polygons towards layers that represent finer structures such as lanes or actors' bounding boxes. Important rasterization parameter is pixel resolution, which we set to $0.1m$ considering the trade-off between image size and ability to represent fine details.

As discussed earlier, we are interested in representing context around each actor separately. To represent context around the i -th actor tracked at time step t_j we create a rasterized image I_{ij} of size $n \times n$ such that the actor is positioned at pixel (w, h) within I_{ij} , where w represents width and h height measured from the bottom-left corner of the image. The image is rotated such that actor's heading points up, where lane directions are computed relative to the actor's heading and then encoded in the HSV space. We set $n = 300$, actor of interest is positioned at $w = 150$ and $h = 50$, so that $25m$ of context in front of the actor and $5m$ from the back is taken into account. Lastly, we color the actor of interest differently so that the vehicle for which we predict trajectory is distinguishable from other vehicles (as seen in Figure 1 it is colored red while other actors are colored yellow).

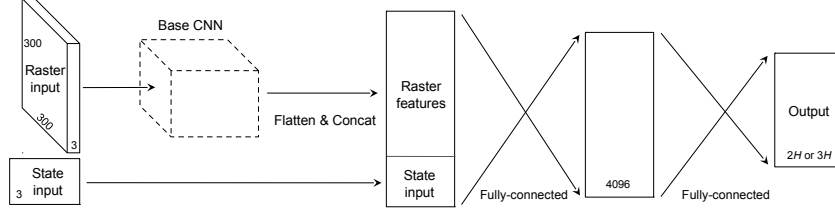


Figure 2: The proposed network architecture combining raster and state inputs

To represent actors' histories, their bounding boxes at consecutive time steps $[t_{j-K+1}, \dots, t_j]$ are rasterized in the raster image on top of map vector layers. Each historical actor polygon is rasterized with the same color as the current polygon yet with reduced level of brightness, resulting in the *fading* effect. Brightness level at t_{j-k} is equal to $\max(0, 1 - k \cdot \delta)$, $k = 0, 1, \dots, K - 1$, where we set $\delta = 0.1$ and K to either 1 (no fading) or 5 (with fading, example shown in Figure 1).

3.2 Optimization problem

To obtain analytical expressions for loss functions used to optimize deep networks, let us first introduce *displacement error* for the i -th actor at time t_j for horizon $h \in \{1, \dots, H\}$,

$$d_{i(j+h)} = \sqrt{(x_{i(j+h)} - \hat{x}_{i(j+h)}(\mathcal{S}_j, \mathcal{M}, \theta))^2 + (y_{i(j+h)} - \hat{y}_{i(j+h)}(\mathcal{S}_j, \mathcal{M}, \theta))^2}, \quad (1)$$

defined as Euclidean distance between observed and predicted positions. Here, θ denotes parameters of a model, while $\hat{x}_{i(j+h)}(\mathcal{S}_j, \mathcal{M}, \theta)$ and $\hat{y}_{i(j+h)}(\mathcal{S}_j, \mathcal{M}, \theta)$ denote position outputs of the model that takes available states \mathcal{S}_j and map \mathcal{M} as inputs. Then, overall loss incurred by predicting trajectory for a complete prediction horizon is equal to average squared displacement error of trajectory points,

$$L_{ij} = \frac{1}{H} \sum_{h=1}^H d_{i(j+h)}^2, \quad (2)$$

where we train the model to output $2H$ -dimensional vector, representing predicted x - and y -positions for each of H trajectory points. Optimizing over all actors and time steps found in the training data, we find optimal parameters by minimizing overall training loss,

$$\theta^* = \arg \min_{\theta} \mathcal{L} = \arg \min_{\theta} \sum_{j=1}^T \sum_{i=1}^{N_j} L_{ij}. \quad (3)$$

Alternatively, as the prediction task is inherently noisy it is useful to capture aleatoric uncertainty present in the data [16, 21], in addition to optimizing for point estimate as in (3). To that end, we assume that displacement errors are sampled from a half-normal distribution [14], denoted as

$$d_{i(j+h)} \sim \mathcal{FN}(0, \hat{\sigma}_{i(j+h)}(\mathcal{S}_j, \mathcal{M}, \theta)^2), \quad (4)$$

where standard deviation $\hat{\sigma}_{i(j+h)}$ is computed by the model. Then, we can write overall loss for the i -th actor at time t_j as negative log-likelihood of the observed data, equal to

$$L_{ij} = \sum_{h=1}^H \left(\frac{d_{i(j+h)}^2}{2 \hat{\sigma}_{i(j+h)}(\mathcal{S}_j, \mathcal{M}, \theta)^2} + \log \hat{\sigma}_{i(j+h)}(\mathcal{S}_j, \mathcal{M}, \theta) \right), \quad (5)$$

where we train the model to output $3H$ -dimensional vector, representing predicted x -position, y -position, and standard deviation of error for each of H trajectory points. Lastly, optimizing over entire training data we solve (3) with L_{ij} computed as in (5).

3.3 Network architecture

In this section we describe an architecture used to solve the optimization problems (2) and (5), which we also illustrate in Figure 2. To extract features from an input raster we can use any existing CNN architecture (referred to as *base CNN*). In addition, to input actor state we encode it as a 3-D vector comprising velocity, acceleration, and heading change rate (position and heading are not required as they were already used during raster generation), and concatenate the resulting vector with flattened output of the base CNN. Then, the combined features are passed through a fully-connected layer (we set its size to 4,096) connected to an output layer of size $2H$ if solving (2), or $3H$ if solving (5).

Table 1: Comparison of average prediction errors for competing methods (in meters)

Predictor	Raster	State	Loss	Displacement	Along-track	Cross-track
UKF	–	–	–	2.36	2.69	0.49
AlexNet	w/o fading	no	(2)	3.14	3.11	0.35
AlexNet	w/ fading	no	(2)	1.24	1.23	0.22
AlexNet	w/o fading	yes	(2)	0.97	0.94	0.21
AlexNet	w/ fading	yes	(2)	0.86	0.83	0.20
VGG-19	w/ fading	yes	(2)	0.77	0.75	0.19
ResNet-50	w/ fading	yes	(2)	0.76	0.74	0.18
MobileNet-v2	w/ fading	yes	(2)	0.73	0.70	0.18
MobileNet-v2	w/ fading	yes	(5)	0.71	0.68	0.18

4 Experiments

Baseline We used Unscented Kalman filter (UKF) [40] with dynamic vehicle model [19] as a strong non-CNN baseline, taking raw sensor data from camera, lidar, and radar and outputting state estimates for each tracked vehicle. The tracking filter was readily available as it is a default tracker on our fleet, is pretrained on large amount of labeled data, is highly optimized and successfully tested on millions on driven miles (unfortunately, no other details can be given due to confidentiality concerns). Then, we can use this tracker to predict future motion by forward propagating estimated states in time.

Data We collected 240 hours of data by manually driving AV in Pittsburgh, PA and Phoenix, AZ in various traffic conditions (e.g., varying times of day, days of the week), with data collection rate of $10Hz$ (the same frequency the UKF was run on). Each tracked actor at each discrete tracking time step amounts to a single data point, with overall data comprising 7.8 million data points. We considered prediction horizon of $3s$ (i.e., we set $H = 30$), and used 3:1:1 split to obtain train/validation/test data.

Models We compared the baseline to several variants of the proposed approach. We trained and evaluated the following base CNNs: AlexNet [20], VGG-19 [35], ResNet-50 [13], and MobileNet-v2 (MNv2) [30]. Furthermore, to evaluate how varying input complexity affects performance we considered architectures that use: 1) raster without fading and state, solving (2); 2) raster with fading and without state, solving (2); 3) raster without fading and with state, solving (2); 4) raster with fading and state, solving (2); 5) raster with fading and state, and outputting uncertainty, solving (5).

Training Models were implemented in TensorFlow [1] and trained on 16 Nvidia Titan Xs connected using commodity network hardware. To coordinate the GPUs we used open-source distributed framework Horovod [32], completing training in around 24 hours. We used batch size of 32 and trained with Adam optimizer [17], where we set initial learning rate to 10^{-4} that is further decreased by a factor of 0.9 every 20 thousand iterations. All models were trained end-to-end from scratch, except for a model with uncertainty outputs which was initialized with a corresponding model without uncertainty and then fine-tuned (training from scratch did not give satisfactory results). We deployed models to an AV with an undisclosed GPU aboard, performing batch inference in $10ms$ on average.

4.1 Results

In Table 1 we report error metrics averaged over the prediction horizon that are relevant for motion prediction: displacement errors, as well as along-track and cross-track errors [10].

We first conducted an ablation study using AlexNet, performing a sequence of experiments with varying input complexity (given in the upper half of Table 1). When we provide neither fading nor state inputs the model performs worse than UKF, as the network does not have enough information to estimate current state of an actor from the raster itself. Interestingly, when we include fading the model starts to outperform the baseline by a large margin, indicating that actor’s state can be inferred solely from providing past positions through fading. If instead of fading we directly provide state estimates we get even better performance, as the state info is already distilled and does not have to be estimated from raster. Furthermore, using raster with fading together with state inputs leads to additional performance boost, suggesting that fading carries additional information not available through state itself, and that raster image and other external inputs can be seamlessly combined through the proposed architecture to obtain improved accuracy.

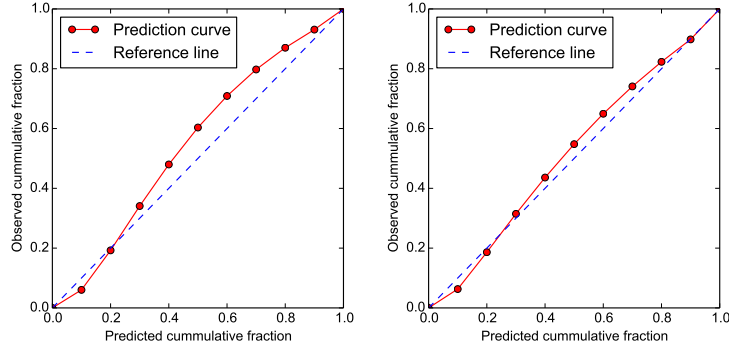


Figure 3: Reliability diagrams at the prediction horizon of: (a) 1 second; (b) 3 seconds

Next, we run experiments with several popular CNN architectures as base CNNs. We found that VGG and ResNet provide improvements over the baseline AlexNet, as observed in other applications as well [35]. However, both are outperformed by the novel MNv2 architecture that combines a number of deep learning ideas under one roof (e.g., bottleneck layers, residual connections, depthwise convolutions). Lastly, taking the best performing MNv2 as base and adding uncertainty outputs led to the best results. Not only do additional outputs allow estimation of trajectory uncertainty in addition to trajectory point estimates, but they also help mitigate the adverse effect of noisy data points during training. In the following we analyze results of this best performing model in greater detail.

We used reliability diagrams to evaluate how closely predicted error distribution matches testing error distribution. The diagrams are generated by measuring how large is an observed displacement error compared to a predicted confidence, and computing what fraction of observed errors falls within the expected range given by the estimated standard deviation. For example, due to the assumption of Gaussianity we expect 68% of observed errors to be within the predicted one sigma, and diagram point at predicted value of 0.68 should be as close as possible to observed value of 0.68. Thus, closer the curve is to the diagonal line, better calibrated is the model. Figure 3 shows the diagrams for prediction horizons of 1s and 3s. The predicted uncertainties are well aligned with the reference line, especially for the 3s-predictions while 1s-predictions are slightly underconfident. Thus, given an estimated sigma output, we can expect with high confidence that in 68% of cases the actual error will not be larger than that value. Plots for other horizons are omitted as they resemble the ones shown.

4.2 Case studies

In the three rows of Figure 4 we give example outputs for three interesting scenes commonly encountered in traffic. As we will see, in all three cases the model provided accurate short-term trajectories as well as reasonable and intuitive uncertainty estimates.

The first case (shown in the first row) involves actor cutting over opposite lane when entering from off-street parking, where the model correctly predicts that the actor will queue for vehicles in front (see the image in the first column). The uncertainty estimates reflect peculiarity of the situation (see the image in the second column), as the actor is not following common traffic rules and may choose to either queue for the leftmost vehicle or continue to cut the road to queue for the vehicles in the other lanes. In the second row we see an actor making a right turn in an intersection, where the model correctly predicts that the actor is planning to enter its own lane. However, uncertainty increases compared to the first example, as the vehicle has higher speed as well as heading change rate, and there is a possibility it may enter any of the two vacant lanes. Lastly, in the third row we have a fast actor going straight, while changing lanes to avoid an obstacle in its current lane. The lane change is correctly predicted, as well as lower cross-track uncertainty due to actor’s higher speed. Quite intuitively, probability that the actor hits the obstacle is estimated at near-zero.

We conducted deeper analysis of the model behavior in the above three cases. First, we performed dropout analysis to estimate epistemic uncertainty in the model itself [16], by dropping out 50% of randomly selected weights in the fully-connected layers, repeating the process 100 times, and visualizing variance of the resulting trajectory points. The results are shown in the third column

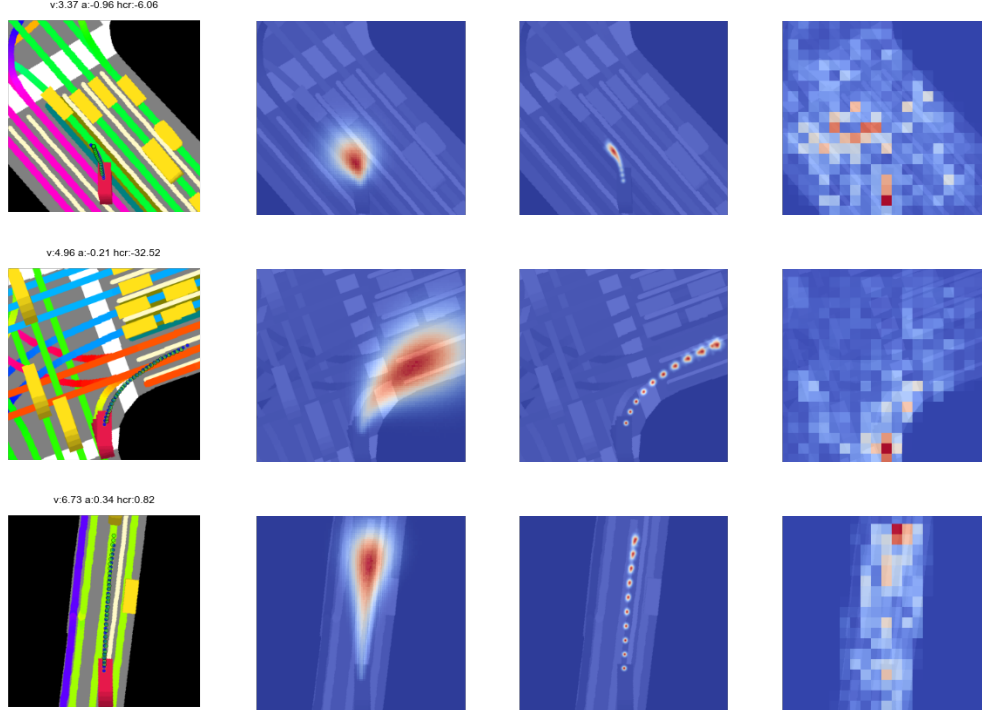


Figure 4: Analysis of the best performing model for three case studies, with results overlaid over input raster images; first column shows ground truth (dotted green line) and predicted trajectory (dotted blue line), second column shows aleatoric uncertainty output by the model, third column shows epistemic uncertainty estimated by dropout analysis, fourth column shows relevant parts of raster estimated by occlusion sensitivity analysis; state inputs are provided above rasters in the first column, indicating velocity (v) in m/s , acceleration (a) in m/s^2 , heading change rate (hcr) in deg/s

of Figure 4, where we see that epistemic uncertainty is very low in all cases, in fact several orders of magnitude lower than aleatoric uncertainty visualized in the second column of Figure 4. This indicates that the model converged, that adding more data would have limited effect on performance, and that the overall uncertainty can be approximated by considering only the learned uncertainty.

Furthermore, we performed occlusion sensitivity analysis to better understand which parts of the raster the model is focusing on during inference [44]. To do so we swept an 15×15 black box across the raster and visualized the amount of change in the output compared to a non-occluded raster (as measured by the average displacement error), with results shown in the fourth column of Figure 4. In the first case the model focuses on the oncoming lane and vehicles in front of the actor, as those parts of the raster are most relevant for a vehicle cutting across oncoming traffic and queuing. Quite intuitively, in the second case the model focuses on nearby vehicles and the crosswalks in the turn lane, while in the third case it focuses on the obstacle and the lane further ahead due to actor’s higher speed. Such analysis helps debug and understand what the model learned, and confirms it managed to extract knowledge from the training data that comes natural to experienced human drivers.

5 Conclusion

We presented an efficient and effective solution to a critical part of the AV problem, prediction of future motion of traffic actors. We introduced a deep learning-based methodology that provides both point estimates of future actor positions and their uncertainty, allowing for deeper understanding of traffic state. The proposed method is based on rasterization of each actor’s context, followed by training of deep convolutional networks to use the resulting raster images to predict actor’s trajectory and its corresponding uncertainty. Extensive evaluation of the methodology strongly suggests its practical benefits, and the framework was subsequently deployed to a fleet of autonomous vehicles.

References

- [1] M. Abadi, A. Agarwal, P. Barham, E. Brevdo, et al. TensorFlow: Large-scale machine learning on heterogeneous systems, 2015.
- [2] A. Alahi, K. Goel, et al. *Social LSTM: Human Trajectory Prediction in Crowded Spaces*. IEEE, Jun 2016.
- [3] L. Ballan, F. Castaldo, A. Alahi, F. Palmieri, and S. Savarese. *Knowledge Transfer for Scene-Specific Motion Prediction*, page 697–713. Springer International Publishing, 2016.
- [4] L. J. Blincoe, T. R. Miller, E. Zaloshnja, and B. A. Lawrence. The economic and societal impact of motor vehicle crashes, 2010 (revised). Technical Report DOT HS 812 013, National Highway Traffic Safety Administration, May 2015.
- [5] A. Z. Broder, P. Ciccolo, et al. Search advertising using web relevance feedback. In *Proceedings of the 17th ACM Conference on Information and Knowledge Management*, pages 1013–1022. ACM, 2008.
- [6] S. Chen. Kalman filter for robot vision: a survey. *IEEE Transactions on Industrial Electronics*, 59(11):4409–4420, 2012.
- [7] A. Cosgun, L. Ma, et al. Towards full automated drive in urban environments: A demonstration in gomentum station, california. In *IEEE Intelligent Vehicles Symposium*, pages 1811–1818, 2017.
- [8] L. Fletcher, S. Teller, et al. *The MIT – Cornell Collision and Why It Happened*, page 509–548. Springer Berlin Heidelberg, 2009.
- [9] K. Fragkiadaki, P. Agrawal, et al. Learning visual predictive models of physics for playing billiards. In *International Conference on Learning Representations (ICLR)*, 2016.
- [10] C. Gong and D. McNally. A methodology for automated trajectory prediction analysis. In *AIAA Guidance, Navigation, and Control Conference and Exhibit*, 2004.
- [11] I. Goodfellow, Y. Bengio, and A. Courville. *Deep Learning*. MIT Press, 2016.
- [12] Y. N. Harari. Reboot for the ai revolution. *Nature News*, 550(7676):324, 2017.
- [13] K. He, X. Zhang, S. Ren, and J. Sun. Deep residual learning for image recognition. In *Proceedings of the IEEE conference on computer vision and pattern recognition*, pages 770–778, 2016.
- [14] N. L. Johnson. The folded normal distribution: Accuracy of estimation by maximum likelihood. *Technometrics*, 4(2):249–256, 1962.
- [15] R. E. Kalman. A new approach to linear filtering and prediction problems. *Transactions of the ASME–Journal of Basic Engineering*, 82(Series D):35–45, 1960.
- [16] A. Kendall and Y. Gal. What uncertainties do we need in bayesian deep learning for computer vision? In *Advances in Neural Information Processing Systems*, 2017.
- [17] D. P. Kingma and J. Ba. Adam: A method for stochastic optimization. *arXiv preprint arXiv:1412.6980*, 2014.
- [18] K. M. Kitani, B. D. Ziebart, J. A. Bagnell, and M. Hebert. *Activity Forecasting*, page 201–214. Springer Berlin Heidelberg, 2012.
- [19] J. Kong, M. Pfeiffer, G. Schildbach, and F. Borrelli. Kinematic and dynamic vehicle models for autonomous driving control design. In *Intelligent Vehicles Symposium (IV), 2015 IEEE*, pages 1094–1099. IEEE, 2015.
- [20] A. Krizhevsky, I. Sutskever, and G. E. Hinton. ImageNet classification with deep convolutional neural networks. In *Advances in neural information processing systems*, pages 1097–1105, 2012.
- [21] B. Lakshminarayanan, A. Pritzel, and C. Blundell. Simple and scalable predictive uncertainty estimation using deep ensembles. In *Advances in Neural Information Processing Systems*, 2017.
- [22] N. Lee, W. Choi, P. Vernaza, C. B. Choy, et al. *DESIRE: Distant Future Prediction in Dynamic Scenes with Interacting Agents*. IEEE, Jul 2017.
- [23] S. Lefèvre, D. Vasquez, and C. Laugier. A survey on motion prediction and risk assessment for intelligent vehicles. *ROBOMECH Journal*, 1(1), Jul 2014.

- [24] NCHS. Health, United States, 2016: With chartbook on long-term trends in health. Technical Report 1232, National Center for Health Statistics, May 2017.
- [25] NHTSA. Early estimate of motor vehicle traffic fatalities for the first half (jan–jun) of 2017. Technical Report DOT HS 812 453, National Highway Traffic Safety Administration, December 2017.
- [26] G. Nuti, M. Mirghaemi, P. Treleaven, and C. Yingsaeree. Algorithmic trading. *Computer*, 44(11):61–69, 2011.
- [27] P. Ondruška, J. Dequaire, D. Z. Wang, and I. Posner. End-to-end tracking and semantic segmentation using recurrent neural networks. *arXiv preprint arXiv:1604.05091*, 2016.
- [28] P. Ondruška and I. Posner. Deep tracking: Seeing beyond seeing using recurrent neural networks. In *Proceedings of the Thirtieth AAAI Conference on Artificial Intelligence*, pages 3361–3367. AAAI Press, 2016.
- [29] S. E. Polzin. Implications to public transportation of emerging technologies. 2016.
- [30] M. Sandler, A. Howard, M. Zhu, A. Zhmoginov, and L.-C. Chen. Inverted residuals and linear bottlenecks: Mobile networks for classification, detection and segmentation. *arXiv preprint arXiv:1801.04381*, 2018.
- [31] M. Schreier, V. Willert, and J. Adamy. An integrated approach to maneuver-based trajectory prediction and criticality assessment in arbitrary road environments. *IEEE Transactions on Intelligent Transportation Systems*, 17(10):2751–2766, Oct 2016.
- [32] A. Sergeev and M. D. Balso. Horovod: fast and easy distributed deep learning in tensorflow. *arXiv preprint arXiv:1802.05799*, 2018.
- [33] D. Silver, A. Huang, et al. Mastering the game of go with deep neural networks and tree search. *Nature*, 529(7587):484–489, 2016.
- [34] D. Silver, T. Hubert, et al. Mastering chess and shogi by self-play with a general reinforcement learning algorithm. *arXiv preprint arXiv:1712.01815*, 2017.
- [35] K. Simonyan and A. Zisserman. Very deep convolutional networks for large-scale image recognition. *arXiv preprint arXiv:1409.1556*, 2014.
- [36] S. Singh. Critical reasons for crashes investigated in the national motor vehicle crash causation survey. Technical Report DOT HS 812 115, National Highway Traffic Safety Administration, February 2015.
- [37] T. Streubel and K. H. Hoffmann. *Prediction of driver intended path at intersections*. IEEE, Jun 2014.
- [38] E. J. Topol. *The patient will see you now: the future of medicine is in your hands*. Tantor Media, 2015.
- [39] O. Vinyals, A. Toshev, S. Bengio, and D. Erhan. Show and tell: Lessons learned from the 2015 mscoco image captioning challenge. *IEEE Transactions on Pattern Analysis and Machine Intelligence*, 39(4):652–663, 2017.
- [40] E. A. Wan and R. Van Der Merwe. The unscented kalman filter for nonlinear estimation. In *Adaptive Systems for Signal Processing, Communications, and Control Symposium 2000. AS-SPCC. The IEEE 2000*, pages 153–158. Ieee, 2000.
- [41] J. Wang, D. Fleet, and A. Hertzmann. Gaussian process dynamical models for human motion. *IEEE Transactions on Pattern Analysis and Machine Intelligence*, 30(2):283–298, Feb 2008.
- [42] K.-C. Wang and R. Zemel. Classifying nba offensive plays using neural networks. In *Proceedings of MIT Sloan Sports Analytics Conference*, pages 1094–1099, 2016.
- [43] J. Wiest. *Statistical long-term motion prediction*. Universität Ulm, 2017.
- [44] M. D. Zeiler and R. Fergus. Visualizing and understanding convolutional networks. In *European conference on computer vision*, pages 818–833. Springer, 2014.
- [45] B. D. Ziebart, A. Maas, J. A. Bagnell, and A. K. Dey. Maximum entropy inverse reinforcement learning. In *Proceedings of the 23rd national conference on Artificial intelligence-Volume 3*, pages 1433–1438. AAAI Press, 2008.
- [46] J. Ziegler, P. Bender, M. Schreiber, et al. Making bertha drive—an autonomous journey on a historic route. *IEEE Intelligent Transportation Systems Magazine*, 6:8–20, 10 2015.